



Impact of Inclined Lorentz Force and Schmidt Number on Chemically Reactive Newtonian Fluid Flow on a Stretchable Surface When Stefan Blowing and Thermal Radiation are Significant

U. S. Mahabaleshwar¹ · T. Anusha¹ · P. H. Sakanaka² · Suvanjan Bhattacharyya³

Received: 19 December 2020 / Accepted: 1 July 2021 / Published online: 25 July 2021
© King Fahd University of Petroleum & Minerals 2021

Abstract

The influence of inclined magnetic field and heat and mass transfer of a hydromagnetic fluid on stretching/shrinking sheet with Stefan blowing effects and radiation has been investigated. The elementary viscous equations for momentum, heat and mass transfer, which are highly nonlinear partial differential equations, are mapped into highly nonlinear ordinary differential equations with the help of similarity transformation. The subsequent highly nonlinear differential equation is solved analytically. The exact solution of heat and mass transfer appearances is found in terms of the incomplete gamma function. The species and temperature boundary conditions are assumed to be a linear function of the distance from the origin. Further, the impact of various parameters, such as Chandrasekhar number, thermal radiation, inclined Lorentz force and mass transpiration on velocity and temperature summaries, are conferred in detail.

Keywords Radiation · Stefan blowing effects · Inclined MHD · Differential equation · Analytical solution · Mass transpiration

Abbreviations

Symbols

a	Constant
B_0	Magnetic field (Wm^{-2})
C	Species concentration (mol m^{-3})
C_w	Species concentration at the wall (mol m^{-3})
C_∞	Ambient species concentration (mol m^{-3})
f	Similarity variable for velocity

k^*	Mean absorption coefficient (m^{-2})
N_R	$\left(= \frac{16\sigma^* T_\infty^3}{3k^* K} \right)$ Radiation parameter
p	Pressure of the fluid
Pr	$\left(= \frac{\nu}{\alpha} \right)$ Prandtl number
Q	$\left(= \frac{\sigma B_0^2}{a\rho} \right)$ Constant magnetic parameter
q_r	Radiative heat flux
q_w	Surface heat flux from the plate (Wm^{-2})
Sc	$\left(= \frac{\nu}{D} \right)$ Schmidt number
T	Fluid temperature (K)
T_∞	Surrounding fluid temperature (K)
T_w	Temperature of the surface (K)
u and v	Velocity components in the x - and y -direction (ms^{-1})
U_w	Velocity of stretching sheet
v_w	Wall blowing velocity (ms^{-1})
x and y	Coordinate systems (m)

✉ Suvanjan Bhattacharyya
suvanjan.bhattacharyya@pilani.bits-pilani.ac.in
U. S. Mahabaleshwar
u.s.m@davangereuniversity.ac.in
T. Anusha
anushat.math@gmail.com
P. H. Sakanaka
sakanaka321@yahoo.com.br

- ¹ Department of Mathematics, Davangere University, Shivagangothri, Davangere 577 007, India
- ² Institute of Physics “Gleb Wataghin”, State University of Campinas, Campinas, SP, Brazil
- ³ Department of Mechanical Engineering, Birla Institute of Technology and Science Pilani, Pilani Campus, Vidya Vihar, Pilani, Rajasthan 333 031, India

Superscript

' Differentiation with respect to η

Greek Symbols

α	Thermal diffusivity of fluid (m^2s^{-1})
β	Constant
Λ	Stefan blowing parameter



ξ	Variable
ζ	Variable
η	Blasius similarity variable
κ	Thermal conductivity of fluid ($\text{Wm}^{-1}\text{K}^{-1}$)
θ	Similarity variable for temperature
λ	Stretching/shrinking parameter
$\lambda > 0$	Stretching sheet
$\lambda < 0$	Shrinking sheet
ν	Kinematic viscosity of fluid (m^2s^{-1})
ρ	Density of fluid (Kgm^{-3})
C_p	Constant pressure specific thermal capacity of the fluid (JK^{-1})
σ	Electrical conductivity of fluid (Sm^{-1})
σ^*	Stefan-Boltzmann constant
τ	Inclined parameter of magnetic field
ϕ	Similarity variable for concentration
Γ	Incomplete gamma function

1 Introduction

In many engineering applications, Newtonian fluid flow due to stretching/shrinking sheet involves the extrusion of plastic sheets and drawing operation of plastic sheets among many things [1–3]. For the processes, for example, drying and purifying methods, where boundaries are perforated, Stefan blowing (wall injection) has significant applications. Stephan problem provides the idea of blowing effect, which is the major implementation of mass transfer of species. The product quality is greatly influenced by heat and mass flow between stretching sheet and flow [4].

A novel work on the boundary-layer flow over a continuously stretching sheet was done by Sakiadis [5]. The work becomes the inspiration for many researchers and motivated them to investigate stretching sheet problems in detail. Exact analytical solution for Navier–Stokes was investigated by Crane [6] and Fang et al. [7]. Banks [8] presented a similarity solution for stretching sheet using numerical and analytical techniques. Magyari and Keller [9] analytically evaluated the two-dimensional flow induced by stretching of permeable wall, and the exact solutions have been derived. Homotopy analysis methods were employed to obtain exact analytic solutions [10].

Carragher and Crane [11] theoretically investigated the thermal transport for a continuously stretching plate and obtained the rate of heat transfer for moderate and large Prandtl number (Pr). Grubka and Bobba [12] employed power-law distribution for temperature in thermal transport in a linearly stretching sheet. Two parameters, namely temperature parameter and Prandtl number, are used to demonstrate the heat transfer behaviour. Dutta et al. [13] analytically investigated flow over a continuously stretching sheet for temperature distribution. Uniform heat flux was given

to a stretching sheet, and velocity of sheet directly depends on the slit distance. It was found that temperature decreases with an increase in Prandtl number.

Other similar work includes [14–16]. Weidman et al. [17] and Ishak et al. [18] explored a similar boundary flow over a moving surface and found dual solutions. The impact of Blasius flow and Sakiadis flow has been investigated for thermal radiation on a viscous boundary layer [19]. A slips model is used to investigate hydromagnetics flow and thermal transfer over expanding or stretching and shrinking surface [20]. Andersson [21–24] reported work related to chemical reaction for stretching plate. Pal and Mondal [25] approved a numerical examination to study the impact of Soret and Dufour, radiation and species on hydromagnetics flow due to stretching/shrinking surface in a porous medium. Khan [26] numerically reported the impact of homogeneous–heterogeneous reactions on the stretching sheet in non-Newtonian fluid and found that velocity of viscoelastic fluid is decreased with an increase in viscoelastic parameters, λ . Bhattacharyya et al. [27] examined the flow of MHD due to a stretching sheet with suction and blowing and reported a reduction in velocity and surge in concentration was observed with an increment in magnetic parameter.

Other studies involve transport of species (or mass transfer and Lorentz forces) [28–30, 44]. Spalding [31] investigated the mass or species transfer in viscous flow over a flat plate, vertical plate and sphere using the Karman–Pohlhausen–Kroujiline method. Recently, Mahabaleshwar et al. [32–39] and Khan et al. [40–43] have investigated analytical examination to impact of different fluids with numerous parameters MHD/porous media flow.

For the objective of the research, we consider the effect of radiation and MHD on Newtonian flow and chemical reaction over a stretching/shrinking sheet with Stefan blowing effects. By means of similarity transformation, the flow equations are mapped from PDEs to ODEs and solved analytically. The exact analytic solution of heat and mass transfer characteristics is obtained in terms of the incomplete gamma function.

2 Mathematical Formulation and Physical Modelled Equations

Laminar, steady two-dimensional motion in the Cartesian coordinate xy -plane on the stretching/shrinking sheet under the effect of inclined MHD, Stefan blowing and radiation has been investigated. The heat and mass impacts are investigated once thermal conductivity varies as a linear function of temperature and concentration. The laminar boundary flow is examined in the presence of radiation and MHD. A steady magnetic field at an angle τ to the positive direction of the y -axis has been applied. Magnetic Reynolds number is considered to be very



small (see Mahabaleshwar 2007, 2008). Further, the concentration and temperature distribution at the sheet and $y \rightarrow \infty$ are assumed to be constants as C_w, T_w, T_∞ and C_∞ , respectively.

The familiar Prandtl equations for two-dimensional flow, heat and mass equations under the boundary-layer approximations are stated as follows:

$$\frac{\partial u}{\partial x} + \frac{\partial v}{\partial y} = 0, \tag{1}$$

$$\rho \left(u \frac{\partial u}{\partial x} + v \frac{\partial u}{\partial y} \right) = -\frac{\partial p}{\partial x} + \mu \left(\frac{\partial^2 u}{\partial x^2} + \frac{\partial^2 u}{\partial y^2} \right) - \sigma B_0^2 \sin^2(\tau) u, \tag{2}$$

$$\rho \left(u \frac{\partial v}{\partial x} + v \frac{\partial v}{\partial y} \right) = -\frac{\partial p}{\partial y} + \mu \left(\frac{\partial^2 v}{\partial x^2} + \frac{\partial^2 v}{\partial y^2} \right), \tag{3}$$

$$u \frac{\partial C}{\partial x} + v \frac{\partial C}{\partial y} = D \left(\frac{\partial^2 C}{\partial x^2} + \frac{\partial^2 C}{\partial y^2} \right), \tag{4}$$

$$\rho C_p \left(u \frac{\partial T}{\partial x} + v \frac{\partial T}{\partial y} \right) = \kappa \left(\frac{\partial^2 T}{\partial x^2} + \frac{\partial^2 T}{\partial y^2} \right) - \frac{\partial q_r}{\partial y}, \tag{5}$$

where u and v are the velocity components in the x - and y -direction, respectively, p the pressure, C and C_∞ the concentrations of species and concentration at infinity, respectively, T and T_∞ the temperature and temperature at infinity, respectively, and $\rho, \mu, \sigma, D, C_p$ and κ are the density, dynamic viscosity, electrical conductivity, mass diffusivity coefficient, constant pressure specific heat capacity and thermal conductivity, respectively.

Imposed conditions for these nonlinear governing equations are:

$$y = 0 \quad u = U_w(x) = \lambda ax, \quad v = v_w, \quad T = T_w, \quad C = C_w$$

$$\text{as } y \rightarrow \infty \quad u \rightarrow 0, \quad T \rightarrow T_\infty, \quad C \rightarrow C_\infty. \tag{6}$$

$u = U_w(x) = \lambda ax$ gives the velocity distribution of sheet. In given expression represents the coordinates along the direction in which sheet is stretching or shrinking, and λ is the constant ($\lambda > 0$ means stretching, $\lambda < 0$ means shrinking and $\lambda = 0$ means surface is permeable).

The Rosseland approach for radiative heat flux is assumed by q_r (see Mahabaleshwar *et al.* 2020),

$$q_r = -\frac{4\sigma^*}{3k^*} \frac{\partial T^4}{\partial y}. \tag{7}$$

The Taylor-series expansion for the fourth power of temperature can be presented as:

$$T^4 = T_\infty^4 + 4T_\infty^3(T - T_\infty) + 6T_\infty^2(T - T_\infty)^2 + \dots \tag{8}$$

In Eq. (8), neglecting the quadratic terms onwards

$$T^4 \cong -3T_\infty^4 + 4T_\infty^3 T. \tag{9}$$

Substituting equation (7) into (9), one can obtain:

$$\frac{\partial q_r}{\partial y} = -\frac{16\sigma^* T_\infty^3}{3k^*} \frac{\partial^2 T}{\partial y^2}. \tag{10}$$

Equation (5) is converted into the subsequent equation (10)

$$u \frac{\partial T}{\partial x} + v \frac{\partial T}{\partial y} = \left(\alpha + \frac{16\sigma^* T_\infty^3}{3\rho C_p k^*} \right) \frac{\partial^2 T}{\partial y^2}. \tag{11}$$

Equations (1)–(5) by using dimensionless variables are given by

$$\psi = (\sqrt{av})xf(\eta), \quad \eta = y\sqrt{\frac{a}{v}},$$

$$u = axf_\eta(\eta), \quad v = -\sqrt{av}f(\eta), \quad \theta(\eta) = \frac{T - T_\infty}{T_w - T_\infty}, \quad \phi(\eta) = \frac{C - C_\infty}{C_w - C_\infty}. \tag{12}$$

The physical stream function ψ is defined as follows:

$$u = \frac{\partial \psi}{\partial y}, \quad v = -\frac{\partial \psi}{\partial x}. \tag{13}$$

Equation (13) satisfies the conservation of mass. Substituting Eq. (12a)–(12b) into Eq. (2) is transformed into:

$$\frac{\partial^3 \psi}{\partial y^3} + \frac{\partial \left(\psi, \frac{\partial \psi}{\partial y} \right)}{\partial(x, y)} - \frac{\sigma B_0^2}{\rho} \sin^2(\tau) \frac{\partial \psi}{\partial y} = 0. \tag{14}$$

In Eq. (14), the second term specifies the Jacobian.

Substituting Eqs. (14) and (10) into Eq. (12b), the following transformed equation with constant coefficient is derived.

The similarity transformation $\psi(x, y) = (\sqrt{av})xf(\eta)$ is presented in Eqs. (2)–(5), which is given in the following equations:

$$f_{\eta\eta\eta} + ff_{\eta\eta} - f_\eta^2 - Q \sin^2(\tau)f_\eta = 0, \tag{15}$$

$$\phi_{\eta\eta} + Sc(f\phi_\eta) = 0, \tag{16}$$

$$(1 + N_R)\theta_{\eta\eta} + Pr(f\theta_\eta) = 0. \tag{17}$$

In these problems, the pressure gradient is negligible.

The appropriate boundary conditions for Eqs. (15) to (17) are given by:

$$f(0) = \Lambda(\phi_\eta)_{\eta=0}, \quad f_\eta(0) = \lambda, \quad \theta(0) = \phi(0) = 1$$

$$f_\eta(\infty) \rightarrow 0, \quad \theta(\infty) = \phi(\infty) \rightarrow 0 \tag{18}$$

where $Q = \frac{\sigma B_0^2}{\rho a}$ is the Chandrasekhar number (\sqrt{Q} is called Hartmann number), λ represents stretching/shrinking

parameter, $\lambda > 0$ for the stretching sheet, $\lambda < 0$ for the shrinking sheet and $\lambda = 0$ for the fixed surface, Λ represents the Stefan blowing due to mass transpiration (suction/injection) and Stefan blowing velocity is given by $v_w = -(\sqrt{a\rho})\Lambda\phi_\eta(0)$, $Sc = \frac{\nu}{D}$ represents the Schmidt number, $Pr = \frac{\nu}{\alpha}$ represents the Prandtl number and $N_R = \frac{16\sigma^*T_\infty^3}{3k^*K}$ represents the thermal radiation (Fig. 1).

3 Methodology for Velocity

The nature of solution in the exact analytical solutions of equations (15) is given by,

$$f(\eta) = \beta - \frac{1}{\beta} \left\{ Q \sin^2(\tau) + \lambda \text{Exp}(-\beta\eta) \right\} \tag{19}$$

and

$$f_\eta(\eta) = \lambda \text{Exp}(-\beta\eta) \tag{20}$$

provided that $\beta > 0$.

Note that

- i) The classical Crane (1970) flow is recovered from Eq. (15) for $Q = 0$, $\lambda = 1$ and $\tau = 90^\circ$.
- ii) The classical Pavlov (1970) flow is recovered from Eq. (15) for $V_C = 0$, $\lambda = 1$ and $\tau = 90^\circ$.
- iii) The Mahabaleshwar et al. (2016) flow is recovered from Eq. (15) for $\lambda = 1$ and $\tau = 90^\circ$.

- iv) The Fang and Zing (2014) flow is recovered from Eq. (15) for $Q = 0$, $\lambda = 1$ and $\tau = 90^\circ$.

4 Methodology for Concentration and Temperature

Substituting Eq. (19) into Eqs. (16) and (17), the mass and temperature equations are transformed, using the relationship $\xi = \frac{Sc}{\beta^2} \exp(-\beta\eta)$ and $\zeta = \frac{Pr}{\beta^2} \exp(-\beta\eta)$, and are converted to:

$$\xi \phi_{\xi\xi} + \left\{ 1 - Sc \left(1 - \frac{1}{\beta^2} Q \sin^2 \tau \right) + \xi \lambda \right\} \phi_\xi = 0 \tag{21}$$

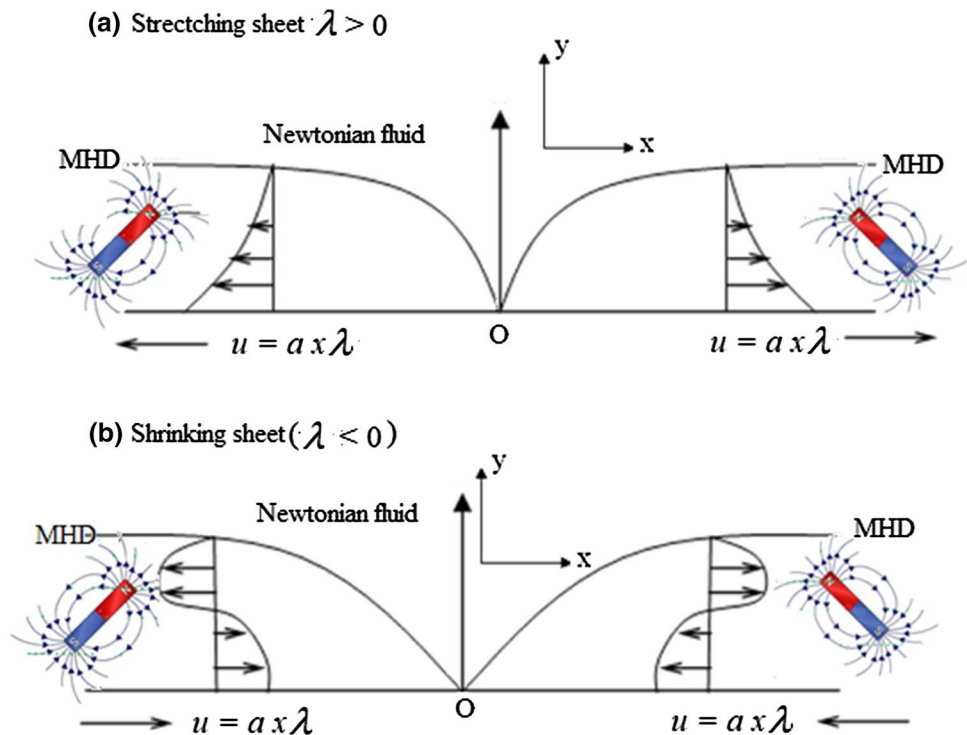
$$(1 + N_R) \zeta \theta_{\zeta\zeta} + \left\{ 1 + N_R - Pr \left(1 - \frac{1}{\beta^2} Q \sin^2 \tau \right) + \zeta \lambda \right\} \theta_\zeta = 0 \tag{22}$$

subject to the corresponding boundary conditions

$$\phi \left(\frac{Sc}{\beta^2} \right) = \theta \left(\frac{Pr}{\beta^2} \right) = 1, \phi(0) = \theta(0) = 0. \tag{23}$$

The final solutions, after further transformations of Eqs. (21) and (22) into incomplete gamma function (Abramowitz and Stegun), are given by

Fig. 1 Pictographic representation of stretching/shrinking boundary



$$\phi(\xi) = \frac{\Gamma\left[Sc\left(1 - \frac{1}{\beta^2}Q\sin^2\tau\right), 0\right] - \Gamma\left[Sc\left(1 - \frac{1}{\beta^2}Q\sin^2\tau\right), \lambda\xi\right]}{\Gamma\left[Sc\left(1 - \frac{1}{\beta^2}Q\sin^2\tau\right), 0\right] - \Gamma\left[Sc\left(1 - \frac{1}{\beta^2}Q\sin^2\tau\right), \lambda\frac{Sc}{\beta^2}\right]}, \quad \phi_\eta(\eta) = -\frac{\beta \exp\left[-\frac{Sc}{\beta^2}\lambda \exp(-\beta\eta)\right]\left(\frac{Sc}{\beta^2}\lambda \exp(-\beta\eta)\right)^{Sc\left(1 - \frac{1}{\beta^2}Q\sin^2\tau\right)}}{\Gamma\left[Sc\left(1 - \frac{1}{\beta^2}Q\sin^2\tau\right), 0\right] - \Gamma\left[Sc\left(1 - \frac{1}{\beta^2}Q\sin^2\tau\right), \lambda\frac{Sc}{\beta^2}\right]}, \tag{24}$$

$$\theta_\eta(\eta) = -\frac{\beta \exp\left[-\frac{Pr}{\beta^2}\frac{\lambda}{1+N_R} \exp(-\beta\eta)\right]\left(\frac{Pr}{\beta^2}\frac{\lambda}{1+N_R} \exp(-\beta\eta)\right)^{\frac{Pr\left(1 - \frac{1}{\beta^2}Q\sin^2\tau\right)}{1+N_R}}}{\Gamma\left[\frac{Pr\left(1 - \frac{1}{\beta^2}Q\sin^2\tau\right)}{1+N_R}, 0\right] - \Gamma\left[\frac{Pr\left(1 - \frac{1}{\beta^2}Q\sin^2\tau\right)}{1+N_R}, \frac{\lambda}{1+N_R}\frac{Pr}{\beta^2}\right]}. \tag{29}$$

The dimensionless concentration and temperature gradients at the sheet are given by

$$\left(\phi_\eta(\eta)\right)_{\eta=0} = -\frac{\beta \exp\left[-\frac{Sc}{\beta^2}\lambda\right]\left(\frac{Sc}{\beta^2}\lambda\right)^{Sc\left(1 - \frac{1}{\beta^2}Q\sin^2\tau\right)}}{\Gamma\left[Sc\left(1 - \frac{1}{\beta^2}Q\sin^2\tau\right), 0\right] - \Gamma\left[Sc\left(1 - \frac{1}{\beta^2}Q\sin^2\tau\right), \lambda\frac{Sc}{\beta^2}\right]}, \tag{30}$$

$$\theta(\zeta) = \frac{\Gamma\left[\frac{Pr\left(1 - \frac{1}{\beta^2}Q\sin^2\tau\right)}{1+N_R}, 0\right] - \Gamma\left[\frac{Pr\left(1 - \frac{1}{\beta^2}Q\sin^2\tau\right)}{1+N_R}, \frac{\lambda}{1+N_R}\zeta\right]}{\Gamma\left[\frac{Pr\left(1 - \frac{1}{\beta^2}Q\sin^2\tau\right)}{1+N_R}, 0\right] - \Gamma\left[\frac{Pr\left(1 - \frac{1}{\beta^2}Q\sin^2\tau\right)}{1+N_R}, \frac{\lambda}{1+N_R}\frac{Pr}{\beta^2}\right]}, \quad \left(\theta_\eta(\eta)\right)_{\eta=0} = -\frac{\beta \exp\left[-\frac{Pr}{\beta^2}\frac{\lambda}{1+N_R}\right]\left(\frac{Pr}{\beta^2}\frac{\lambda}{1+N_R}\right)^{\frac{Pr\left(1 - \frac{1}{\beta^2}Q\sin^2\tau\right)}{1+N_R}}}{\Gamma\left[\frac{Pr\left(1 - \frac{1}{\beta^2}Q\sin^2\tau\right)}{1+N_R}, 0\right] - \Gamma\left[\frac{Pr\left(1 - \frac{1}{\beta^2}Q\sin^2\tau\right)}{1+N_R}, \frac{\lambda}{1+N_R}\frac{Pr}{\beta^2}\right]}. \tag{25}$$

where Γ denotes the incomplete gamma function.

Substituting Eq. (23) into the final solutions of Eqs. (21) and (22) in terms of η , one can obtain:

Using Eq. (19), where $\beta > 0$ represents the root of the equation, solve unknown β and satisfy the equation

$$f(0) = \Lambda\left(\phi_\eta(\eta)\right)_{\eta=0} \tag{32}$$

$$\phi(\eta) = \frac{\Gamma\left[Sc\left(1 - \frac{1}{\beta^2}Q\sin^2\tau\right), 0\right] - \Gamma\left[Sc\left(1 - \frac{1}{\beta^2}Q\sin^2\tau\right), \frac{Sc}{\beta^2}\lambda \exp(-\beta\eta)\right]}{\Gamma\left[Sc\left(1 - \frac{1}{\beta^2}Q\sin^2\tau\right), 0\right] - \Gamma\left[Sc\left(1 - \frac{1}{\beta^2}Q\sin^2\tau\right), \lambda\frac{Sc}{\beta^2}\right]}, \tag{26}$$

$$\theta(\eta) = \frac{\Gamma\left[\frac{Pr\left(1 - \frac{1}{\beta^2}Q\sin^2\tau\right)}{1+N_R}, 0\right] - \Gamma\left[\frac{Pr\left(1 - \frac{1}{\beta^2}Q\sin^2\tau\right)}{1+N_R}, \frac{\lambda}{1+N_R}\frac{Pr}{\beta^2} \exp(-\beta\eta)\right]}{\Gamma\left[\frac{Pr\left(1 - \frac{1}{\beta^2}Q\sin^2\tau\right)}{1+N_R}, 0\right] - \Gamma\left[\frac{Pr\left(1 - \frac{1}{\beta^2}Q\sin^2\tau\right)}{1+N_R}, \frac{\lambda}{1+N_R}\frac{Pr}{\beta^2}\right]}. \tag{27}$$

The first derivatives of concentration and temperature with respect to Blasius similarity variable are as follows:

$$1 - \frac{1}{\beta^2}(\lambda + Q\sin^2\tau) = -\Lambda\frac{\exp\left(-\frac{Sc}{\beta^2}\lambda\right)\left(\frac{Sc}{\beta^2}\lambda\right)^{Sc\left(1 - \frac{1}{\beta^2}Q\sin^2\tau\right)}}{\Gamma\left[Sc\left(1 - \frac{1}{\beta^2}Q\sin^2\tau\right), 0\right] - \Gamma\left[Sc\left(1 - \frac{1}{\beta^2}Q\sin^2\tau\right), \frac{Sc}{\beta^2}\lambda\right]}. \tag{33}$$

Closed-form solutions of Fang and Zing (2014) flow are recovered from Eq. (34) for $Q = 0$, $\lambda = 1$ and $\tau = 90^\circ$.

5 Results and Discussion

The analysis is facilitated in part by systematic mapping of the equations for the velocity, temperature and concentrations, leading to a set of nonlinear ODEs. By employing proper similarity variables, exact analytical solutions for momentum, temperature and concentration profiles are obtained. One has therefore now understood the physics

involved in these interesting dynamics, thanks to the various plots that are generated herein that elaborate on the problem.

Figure 2 represents the influence of Stefan blowing parameters (Λ) on transverse velocity when the stretching boundary (λ) is greater than zero. The Schmidt No. (Sc) is taken unity, while the magnetic field inclination (τ) is 90° . As the Stefan blowing parameter (Λ) is varied between 100, 5, 1 and 0.1, the transverse velocity (η) is increased. It is noted that when the constant magnetic parameter (Q) is 0, the transverse velocity $f(\eta)$ is lower than that when the constant magnetic parameter (Q) is taken as 5. It is also to note that when Q is 0, all the transverse velocity values thus obtained are less than zero. Initially, the transverse velocity

Fig. 2 Influence of Stefan blowing parameter (Λ) on transverse velocity

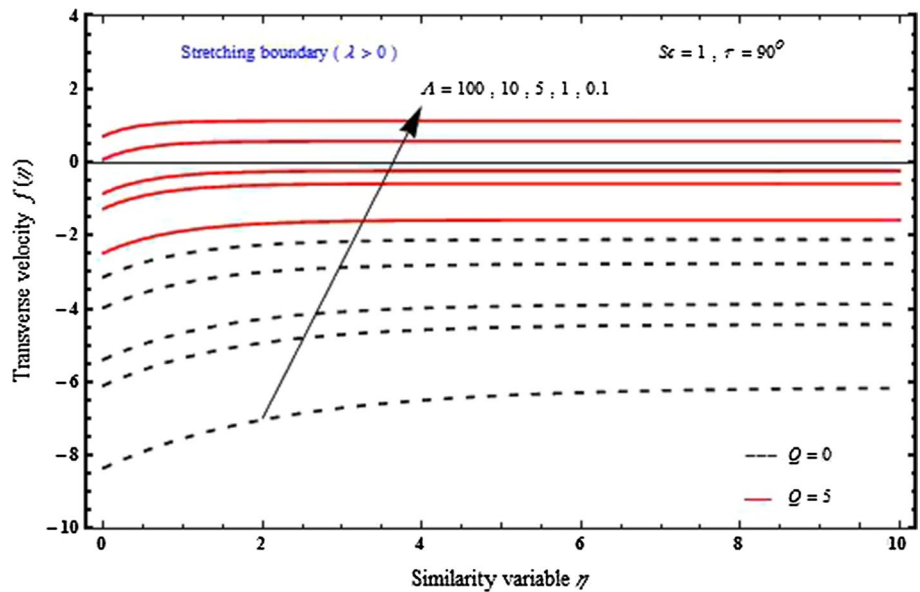
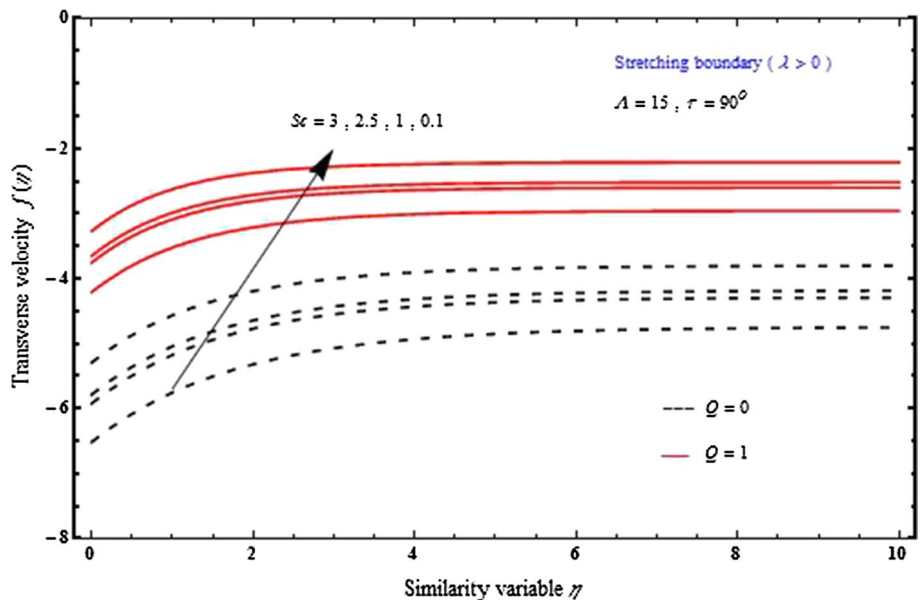


Fig. 3 influence of Schmidt number on transverse velocity



increases when the Blasius similarity variable is increased but becomes constant after some value.

Figure 3 represents the effect of Sc on transverse velocity when the stretching boundary (λ) is greater than zero. The inclined parameter of the magnetic field (τ) is 90° , and the Stefan blowing parameter is 15. Here, the Schmidt number (Sc) is decreased from 3, 2.5, 1 to 0.1. It is seen that when Q is 0 the transverse velocity $f(\eta)$ is below -4 ranging between -4 and -7 and when Q is 1 the transverse velocity ranges between -2 and -4 . Similarly, like Fig. 2, the transverse velocity $f(\eta)$ increases initially when the Blasius similarity variable (η) is increased but finally becomes a constant line.

Figure 4 represents the influence of Stefan blowing parameters on transverse velocity when the shrinking boundary (λ) is less than zero. The Schmidt number (Sc) is taken as 1, and the ‘ Q ’ value has been kept constant at 5. The inclined parameter of the magnetic field (τ) is 90° . As the Stefan blowing parameter (Λ) is varied between 100, 5, 1 and 0.1, the transverse velocity $f(\eta)$ is decreased initially. The transverse velocity $f(\eta)$ ranges from 3 to 2 and becomes constant eventually.

Figure 5 represents the effect of Sc transverse velocity when the stretching boundary (λ) is less than zero. The Stefan blowing parameter (Λ) is kept fixed at 15, and the inclined parameter of the magnetic field (τ) is 90° . The

Fig. 4 Influence of Stefan blowing parameter on transverse velocity

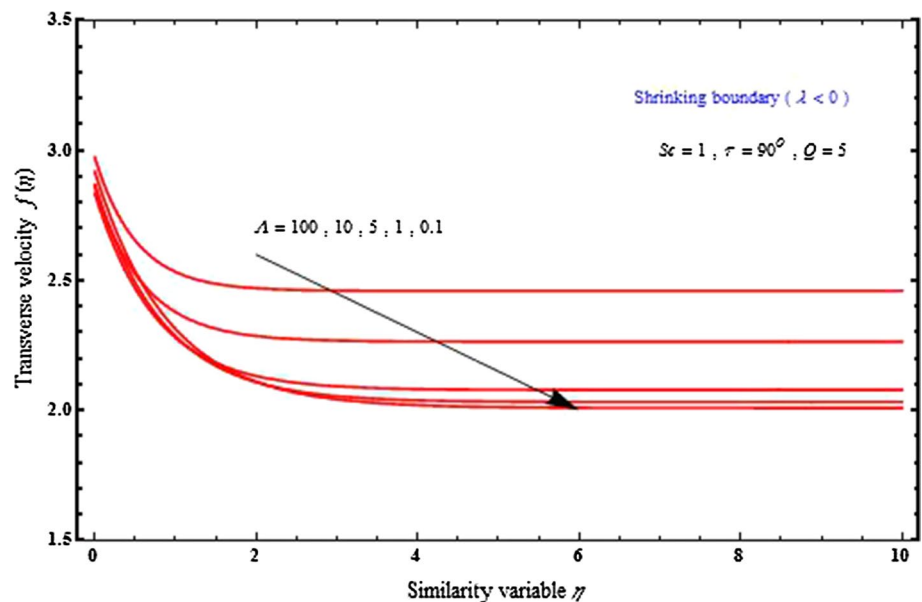


Fig. 5 Influence of Schmidt number on transverse velocity

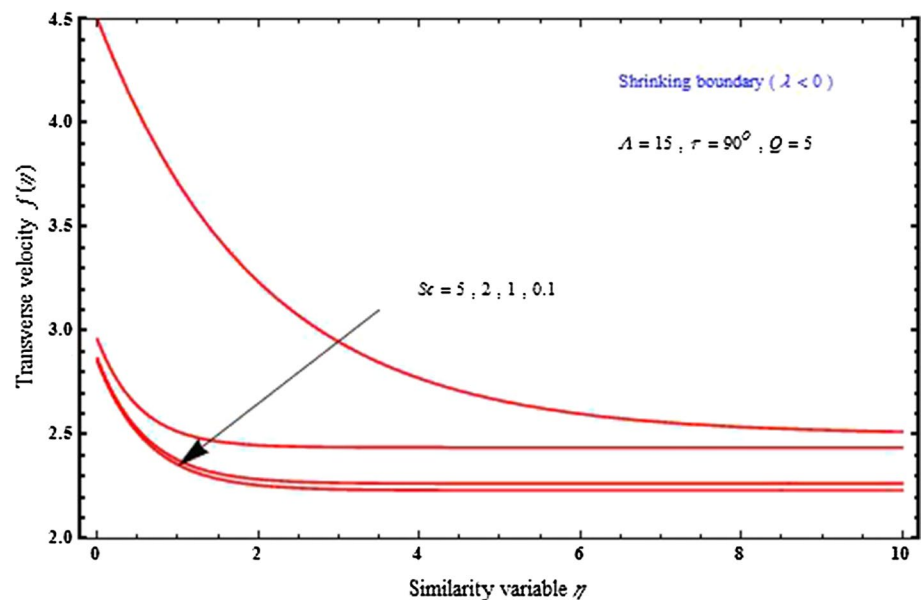
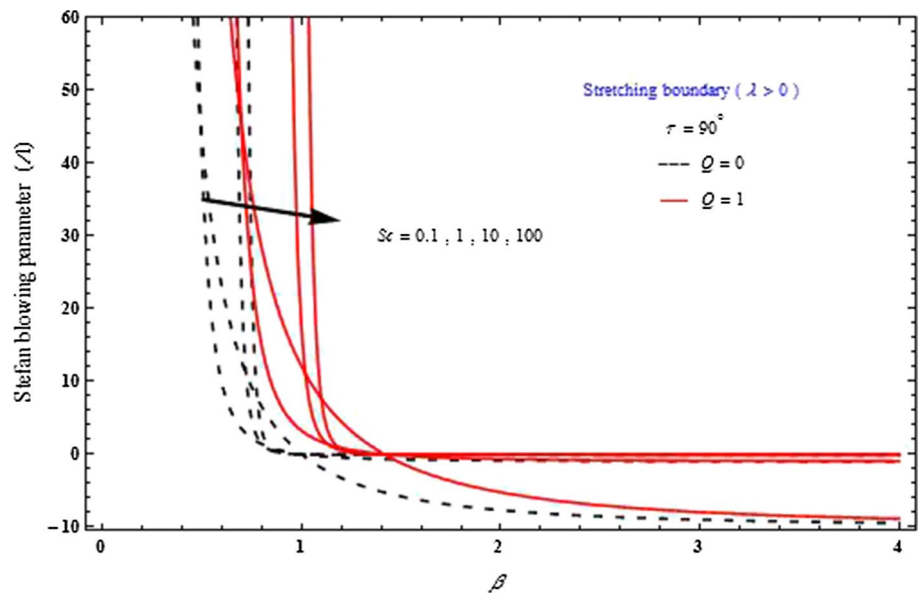


Fig. 6 Influence of Schmidt number on Stefan blowing parameter



constant magnetic parameter (Q) is taken as 5. Now, the Schmidt No. (Sc) is decreased from 5, 2, 1 to 0.1 and so does the corresponding values of transverse velocity $f(\eta)$. It is observed that there are no significant changes in the transverse velocity $f(\eta)$ at higher values of the Blasius similarity variable (η).

Figure 6 represents the influence of Sc on Stefan blowing parameters when the stretching boundary (λ) is greater than zero. Two sets of curves are obtained with constant magnetic parameter (Q) being taken as 0 and 1. The inclined parameter of the magnetic field (τ) is 90° . The Schmidt No. (Sc) is increased from 0.1, 1, 10 to 100 and so the corresponding values of β change. When β is less than 0.5, it is seen that

the Stefan blowing parameter (λ) is infinite. And when the Stefan blowing parameter (λ) is 0, the β value is found to be infinite.

Figure 7 represents the effect of Schmidt number (Sc) on Stefan blowing parameters (λ) when the stretching boundary (λ) is less than zero. For inclined parameter of the magnetic field (τ) of 90° and constant magnetic parameter (Q) of 2, the curves for these Schmidt numbers (Sc s) 0.1, 1, 10 and 100 are obtained. These obtained curves are somewhat similar in nature for inclined parameter of the magnetic field (τ) of 45° and constant magnetic parameter (Q) of 5.

Figure 8 represents the effect of Schmidt number (Sc) on Stefan blowing parameters (λ) and studying the changes in

Fig. 7 Influence of Schmidt on blowing parameter

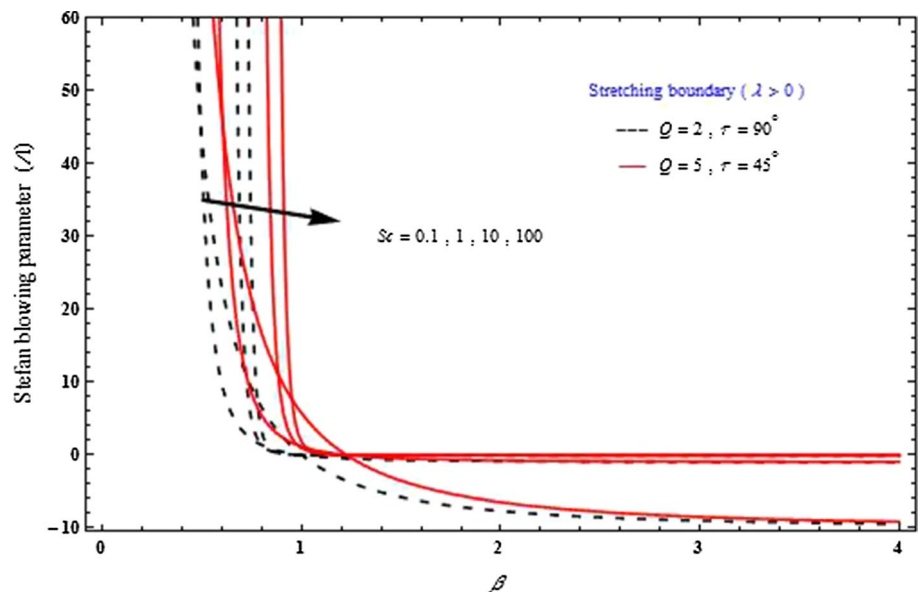
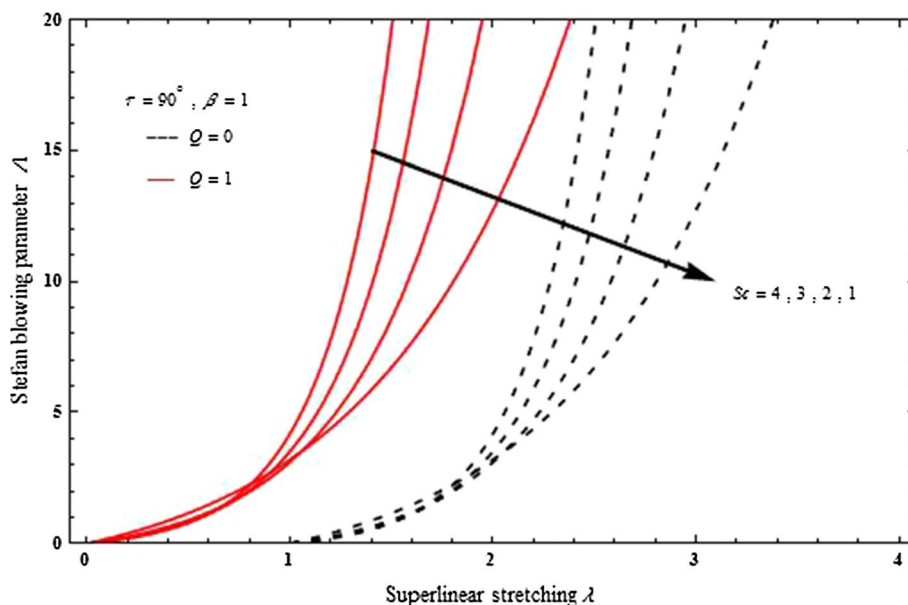


Fig. 8 Influence of Schmidt number on Stefan blowing parameter



super-linear stretching (λ). The inclined parameter of the magnetic field (τ) is 90° . The β value is kept constant at 1. The Schmidt No. (Sc) is decreased from 4, 3, 2 to 1, and the plot obtained seems to be an exponentially increasing graph. As the Schmidt No. (Sc) value decreases, so the rate of increase decreases in the curve plot of (Δ) vs (λ). It is to note that for constant magnetic parameter (Q) value 1, the curves of super-linear stretching (λ) start from 0, while for constant magnetic parameter (Q) value 1, the curves of super-linear stretching (λ) start from 1. Both the sets of curves are somewhat similar.

Figure 9 represents the effect of Sc on Stefan blowing parameters (Δ) by plotting a graph of Stefan blowing

parameter (Δ) vs Chandrasekhar number (Q) when the stretching boundary (λ) is greater than zero with β value kept constant at 1. The Schmidt No. (Sc) is increased from 0.1, 1, 10 to 100, and the plot on Chandrasekhar number (Q) obtained seems to be an exponentially increasing graph. Two sets of curves are obtained with one value ($\lambda = 1$) and another ($\lambda = 2$).

Figure 10 represents the impact of Prandtl number (Pr) on heat transfer flux at the wall ($-\theta_\eta(0)$) with the stretching boundary (λ) greater than 0. The inclined parameter of the magnetic field (τ) is 90° . The β value is varied between 0.2, 0.3, 0.4, 0.5 and 0.6. There are two sets of curves, one set with constant magnetic parameter (Q) and radiation

Fig. 9 Influence of Schmidt number on Stefan blowing parameter

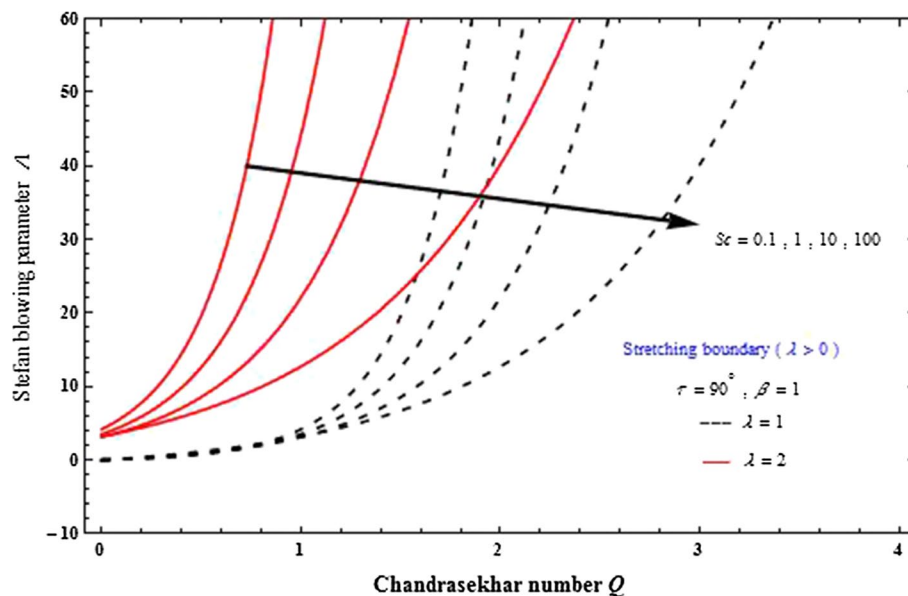


Fig. 10 Influence of β on heat transfer flux at wall

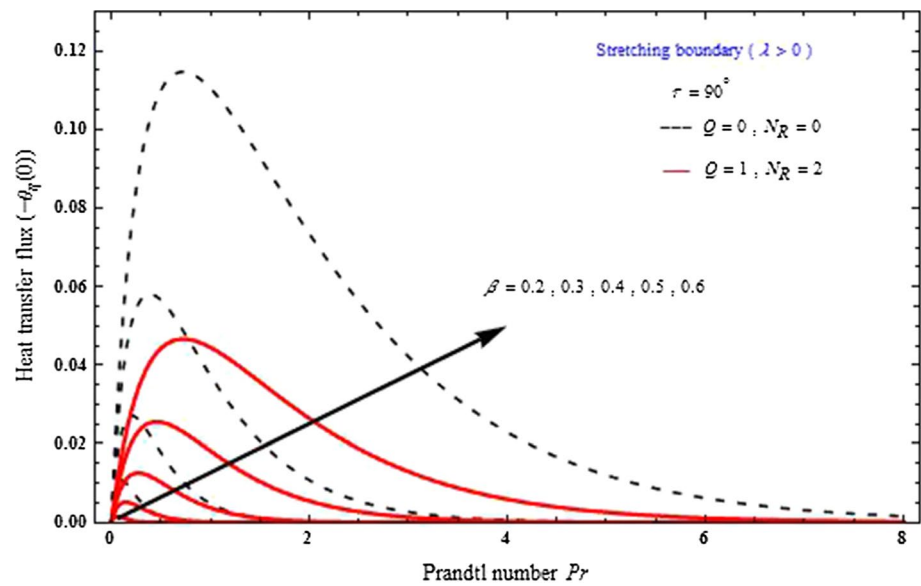
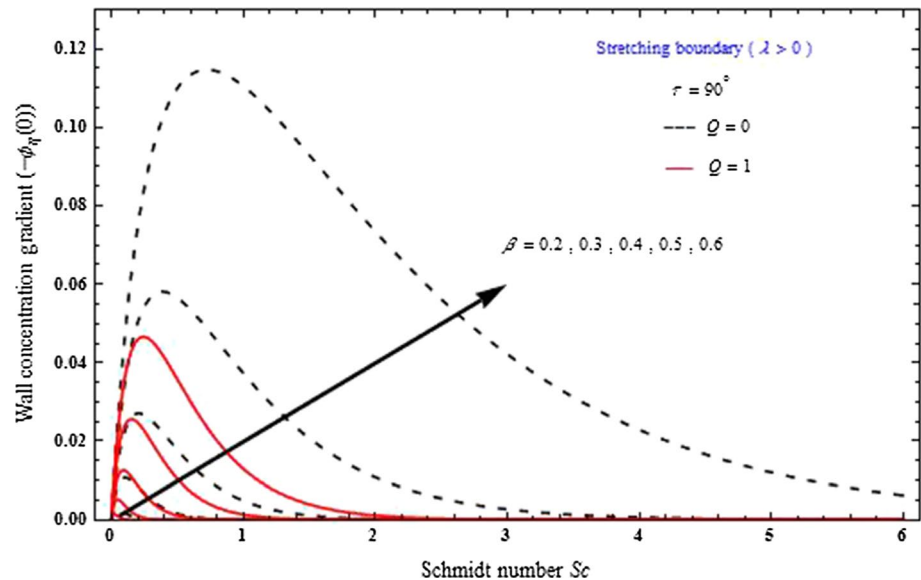


Fig. 11 Influence of β on wall concentration gradient



parameter (N_R) values 0 and 1, respectively, and the other set with (Q) and (N_R) values 0 and 2, respectively. Both of the sets of curves follow a similar pattern. When the Prandtl number (Pr) is increased, the thermal flux at the wall $-\theta_\eta(0)$ value initially increases, reaches a peak value and then decreases. It is to note that when the β value increases, the peak point of the graph also increases.

Figure 11 represents the influence of β on wall concentration gradient $(-\phi_\eta(0))$ with respect to Schmidt number (Sc) with the stretching boundary (λ) greater than 0. The inclined parameter of the magnetic field (τ) is 90° . The β value is varied between 0.2, 0.3, 0.4, 0.5 and 0.6. There are two sets of curves, one with constant magnetic parameter (Q) value 0 and the other set with (Q) value 1. When the Sc is increased, the wall concentration gradient $(-\phi_\eta(0))$ value

initially increases, reaches a peak value and then decreases. It is to note that when the β value increases, the peak point of the graph also increases.

Figure 12 represents the impact of Pr on heat transfer flux at wall $(-\theta_\eta(0))$ with respect to β with the stretching boundary (λ) greater than 0. The inclined parameter of the magnetic field (τ) is 90° . The Pr value is varied between 0.6, 0.5, 0.4, 0.3 and 0.2. There are two sets of curves, one set with constant magnetic parameter (Q) and radiation parameter (N_R) values 0 and 0, respectively, and the other set with (Q) and (N_R) values 1 and 2, respectively. The major portion of the graph follows a linearity (when β greater than 1) and keeps on increasing with a constant rate of increase. When (Q) and (N_R) values are 0 and 0,

Fig. 12 Influence of Prandtl number (Pr) on heat transfer flux at wall

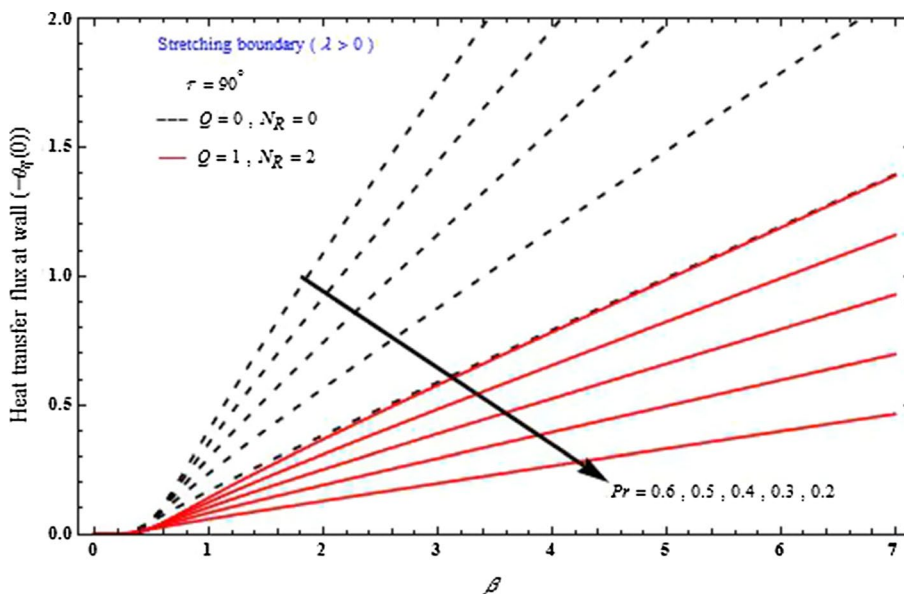
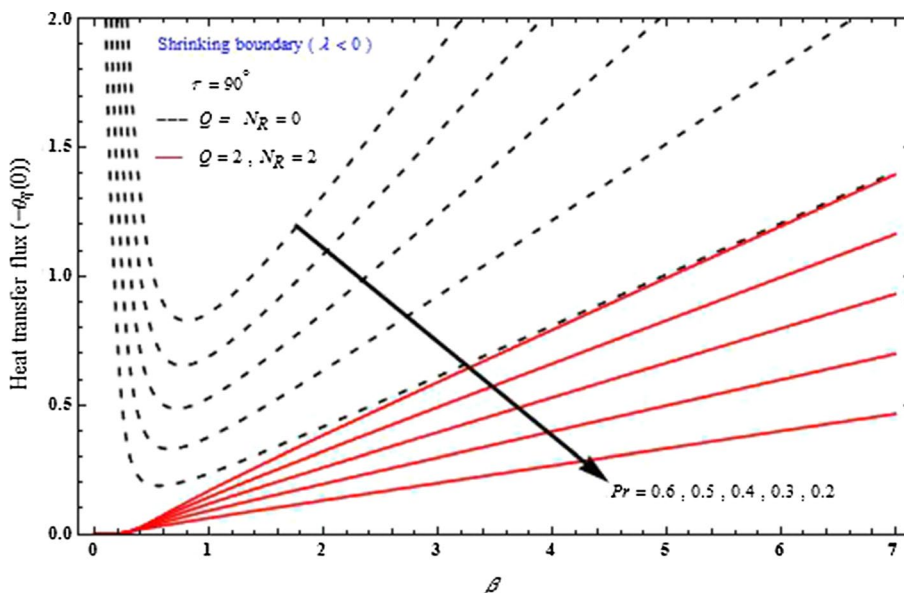


Fig. 13 Influence of Prandtl number (Pr) on heat transfer flux at wall



respectively, the curves are steeper when compared with the other set of data.

Figure 13 represents the impact of Pr on heat transfer flux at wall ($-\theta_\eta(0)$) with respect to β with the stretching boundary (λ) greater than 0. The inclined parameter of the magnetic field (τ) is 90° . The Pr value is varied between 0.6, 0.5, 0.4, 0.3 and 0.2. There are two sets of curves, one set with constant magnetic parameter (Q) and radiation parameter (N_R) values 0 and 0, respectively, and the other set with (Q) and (N_R) values 2 and 2, respectively. When (Q) and (N_R) values are 0 and 0, respectively, the curves plot indicates an infinite value of heat transfer flux at wall ($-\theta_\eta(0)$) with a β around 0 to 1, while these plots drastically change

orientation and become linear when the β value crosses 2. When (Q) and (N_R) values are 2 and 2, respectively, the curves simply follow a linear pattern after β value crosses 1.

Figure 14 represents the influence of Sc on wall concentration gradient with the stretching boundary (λ) greater than 0. The inclined parameter of the magnetic field (τ) is 90° . The Sc value is varied between 0.6, 0.5, 0.4, 0.3 and 0.2. There are two sets of curves, one with constant magnetic parameter (Q) value 0 and the other set with (Q) value 1. When (Q) value is 0, the curves follow a linear pattern after β value crosses 1. And when (Q) value is 1, the linearity is followed after β value crosses 1.5.

Fig. 14 Influence of Schmidt number on wall concentration gradient

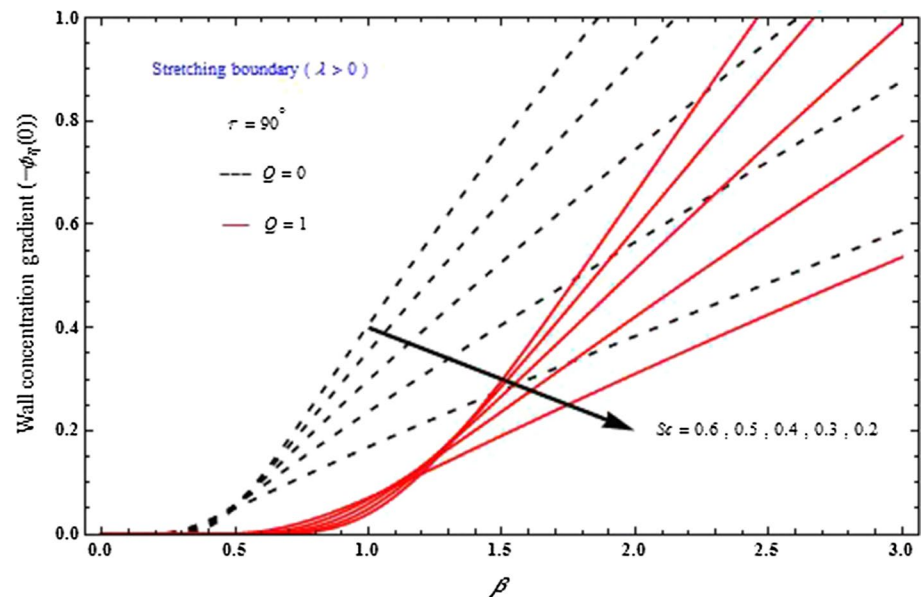


Fig. 15 Influence of Schmidt number on wall concentration gradient

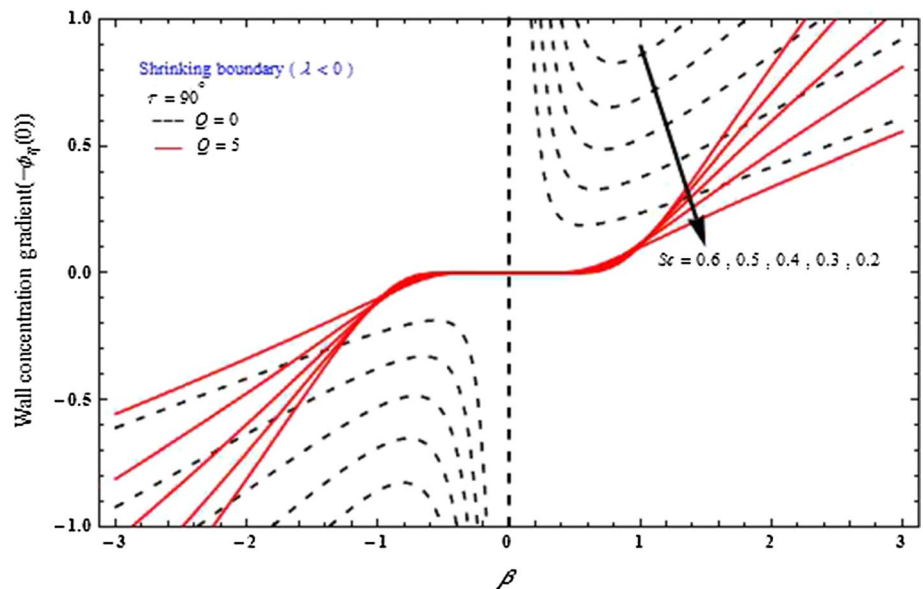


Figure 15 represents the influence of Schmidt number on wall concentration gradient ($-\phi_{\eta}(0)$) with respect to β with the stretching boundary (λ) less than 0. The inclined parameter of the magnetic field (τ) is 90° . The Sc value is varied between 0.6, 0.5, 0.4, 0.3 and 0.2. There are two sets of curves, one with constant magnetic parameter (Q) value 0 and the other set with (Q) value 1. When (Q) value is 0, at $\beta = 0$, for all values of Sc, the wall concentration gradient ($-\phi_{\eta}(0)$) value is infinite, while, for (Q) value 5 at $\beta = 0$, for all values of Sc, the wall concentration gradient ($-\phi_{\eta}(0)$) value is 0. It is to note that, for all taken Scs, below $\beta = 0$, the wall concentration gradient ($-\phi_{\eta}(0)$) value is either 0 or negative for both the (Q) values, while when β is greater than

0 the wall concentration gradient ($-\phi_{\eta}(0)$) value is either 0 or positive.

Figure 16 represents the influence of Stefan blowing parameter on axial velocity $f_{\eta}(\eta)$ with similarity variable (η) with the stretching boundary (λ) greater than 0. The inclined parameter of the magnetic field (τ) is 90° . The Schmidt No. (Sc) value is kept constant at 1. The Stefan blowing parameter (Λ) is varied between 0.1, 1, 5 and 100. It is noted that the axial velocity $f_{\eta}(\eta)$ decreases with an increase in a value of similarity variable (η). For (Q) value 0, the axial velocity $f_{\eta}(\eta)$ becomes zero after similarity variable (η) value 6, while for (Q) value 5, the axial velocity $f_{\eta}(\eta)$ becomes zero after similarity variable (η) value 8.

Fig. 16 Influence of Stefan blowing parameter on axial velocity

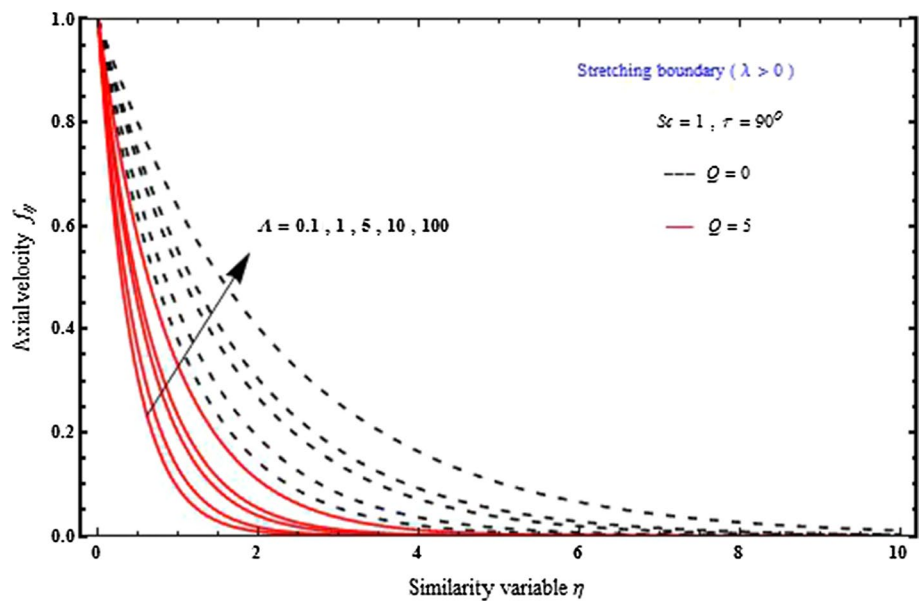


Fig. 17 Influence of Stefan blowing parameter on concentration

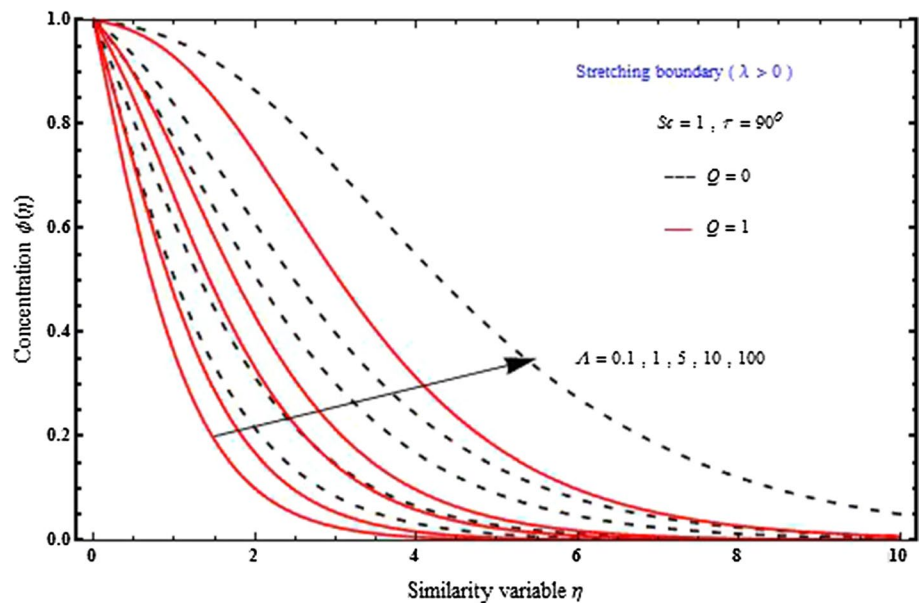


Figure 17 represents the influence of Stefan blowing parameter on concentration $\phi(\eta)$ with respect to similarity variable (η) with the stretching boundary (λ) greater than 0. The inclined parameter of the magnetic field (τ) is 90° . The Schmidt No. (Sc) value is kept constant at 1. The Stefan blowing parameter (λ) is varied between 0.1, 1, 5 and 100. For both the (Q) values, the plot bears resemblance with reverse sigmoid function.

Figure 18 represents the influence of Prandtl number (Pr) on temperature $\phi(\eta)$ with respect to similarity variable (η) with the stretching boundary (λ) greater than 0. The inclined parameter of the magnetic field (τ) is 90° . The Schmidt No. (Sc) value is kept constant at 2. The Stefan blowing

parameter (λ) is also kept constant at 5. The Pr value is varied between 4, 3, 2 and 1. There are two sets of curves, one set with constant magnetic parameter (Q) and radiation parameter (N_R) values 0 and 0, respectively, and the other set with (Q) and (N_R) values 4 and 0.1, respectively. In both the results, the plots are somewhat similar with minimalistic difference. There is a slight similarity in this plot with reverse sigmoid function.

Figure 19 represents the influence of Stefan blowing parameter on temperature $\phi(\eta)$ with respect to similarity variable (η) with the stretching boundary (λ) greater than 0. The inclined parameter of the magnetic field (τ) is 90° . The Schmidt No. (Sc) value is kept constant at 2. The Prandtl

Fig. 18 Influence of Prandtl number (Pr) on temperature

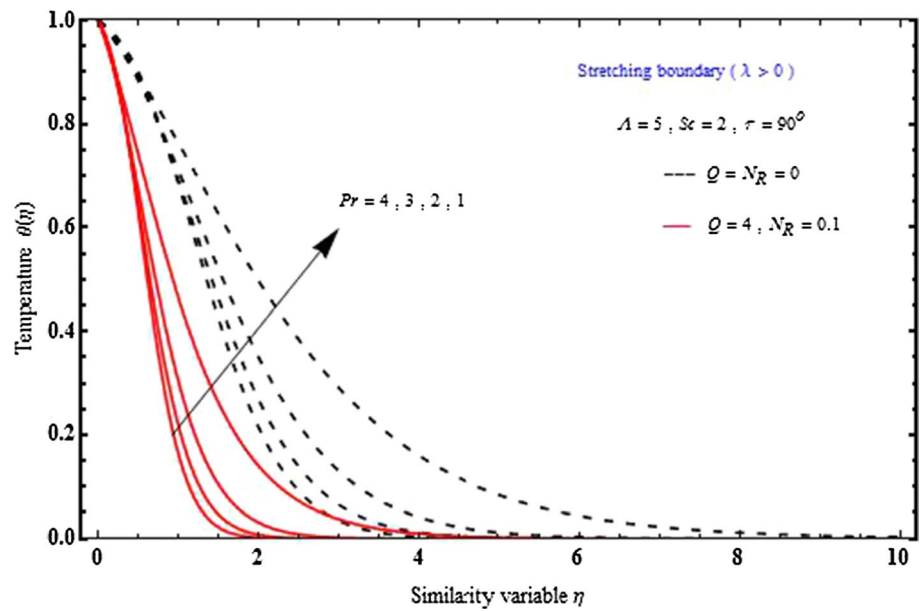
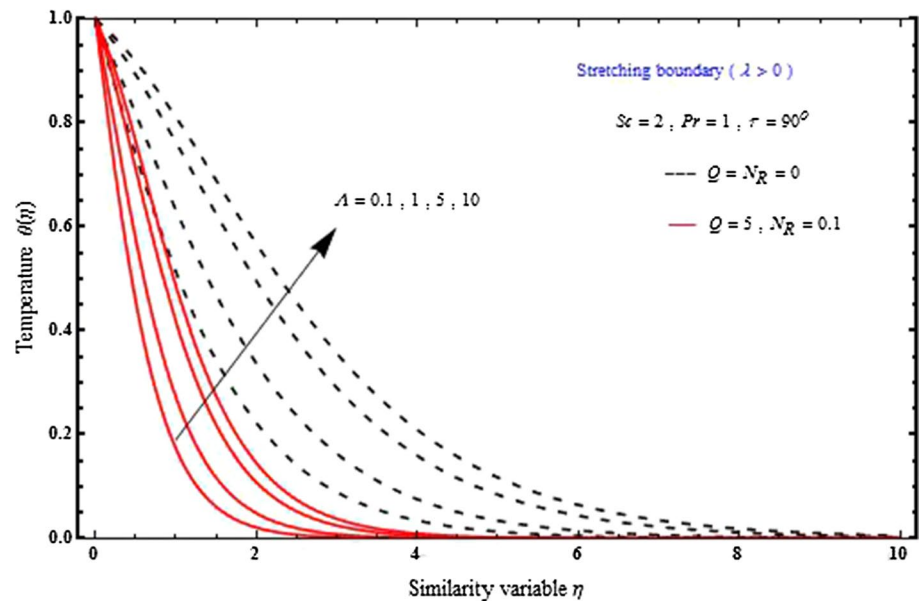


Fig. 19 Influence of Stefan blowing parameter (Λ) on temperature



number (Pr) is also kept constant at 1. The Stefan blowing parameter (Λ) value is varied between 0.1, 1, 5 and 10. There are two sets of curves, one set with constant magnetic parameter (Q) and radiation parameter (N_R) values 0 and 0, respectively, and the other set with (Q) and (N_R) values 5 and 0.1, respectively. In both the results, the plots are somewhat

similar with minimalistic difference. Here, again a slight similarity in this plot with reverse sigmoid function is noted.

Figure 20 represents the influence of Schmidt number (Sc) on temperature $\phi(\eta)$ with respect to similarity variable (η) with the stretching boundary (λ) greater than 0. The inclined parameter of the magnetic field (τ) is 90° . The Stefan blowing parameter (Λ) value is kept constant at 2. The Prandtl number

Fig. 20 Influence of Schmidt number on temperature

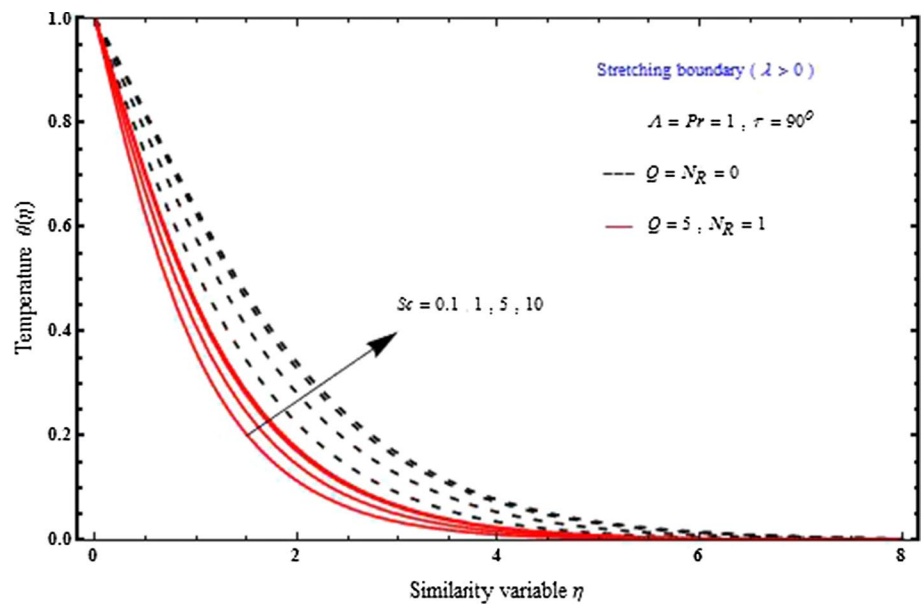


Table 1 Expression for β for various physical parameters

Related works by other authors	Fluids	Value of β
Crane 1970, viscous fluid with suction/injection and without MHD, stretching sheet	Newtonian	$\beta = 1$
Pavlov 1974, incompressible viscous fluid with MHD, stretching sheet without suction/ injection	Newtonian	$\beta = \sqrt{1 + Q}$
Gupta and Gupta 1977, viscous fluid with heat and mass transfer with suction/ injection, stretching sheet	Newtonian	$\beta = \frac{-v_c + \sqrt{v_c^2 + 4(1+Q)}}{2}$
Present work	Newtonian	$f(\eta) = \beta - \frac{1}{\beta} \{ Q \sin^2(\tau) + \lambda \text{Exp}(-\beta\eta) \}$

(Pr) is also kept constant at 1. The Schmidt No. (Sc) value is varied between 0.1, 1, 5 and 10. There are two sets of curves, one set with constant magnetic parameter (Q) and radiation parameter (N_R) values 0 and 0, respectively, and the other set with (Q) and (N_R) values 5 and 1, respectively. In both the results, the plots are somewhat similar with minimalistic difference. Here, again a slight similarity in this plot with reverse sigmoid function is noted. Addition, we mention in Table 1 for different physical parameters of β .

6 Concluding Remarks

The Newtonian fluid flow heat and mass transfer of an incompressible MHD Newtonian fluid over a stretching/shrinking sheet exists for different parameters such as the Stefan blowing parameter, the Chandrasekhar number, inclined angle, the Prandtl number, the wall temperature parameter and the radiation parameter. The exact analytic solution of heat and mass transfer characteristics is

obtained in terms of the incomplete gamma function. The main conclusion derived from the present investigation can be drawn as follows:

- The temperature increases as the Chandrasekhar number (Q) parameter increases, but it decreases as the Prandtl number (Pr) increases.
- Radiation number increases the thermal boundary-layer thickness.
- Increasing radiation parameter heat diffusion is favoured and the temperature increases through the laminar boundary layer.
- Physical/chemical conditions are better suited for effective cooling of the boundary-layer flows.

The present results, industrial application, Newtonian fluid flow due to stretching/shrinking sheet involves the extrusion of plastic sheets, drawing operation of plastic sheets.

Acknowledgements Anusha T. is thankful to Council of Scientific and Industrial Research (CSIR), New Delhi, for financial support in the form of Junior Research Fellowship: File No. 09/1207(0003)/2020-EMR-I.

References

- Altan, T.; Oh, S.; Gegel, H.: Metal Forming Fundamentals and Applications. American Society of Metals, Metals Park (1979)
- Fisher, E.G.: Extrusion of Plastics. Wiley, New York (1976)
- Tadmor, Z.; Klein, I.: Engineering Principles of Plasticating Extrusion. Polymer Science and Engineering Series. Van Nostrand Reinhold, New York (1970)
- Karwe, M.V.; Jaluria, Y.: Numerical simulation of thermal transport associated with a continuous moving flat sheet in materials processing. *ASME J. Heat Transfer* **113**, 612–619 (1991)
- Sakiadis, B.C.: Boundary-layer behavior on continuous solid surface: I Boundary-layer equations for two-dimensional and axisymmetric flow. *J. AIChE* **7**, 26–28 (1961)
- Crane, L.J.: Flow past a stretching plane. *J. Appl. Math. Phys. (ZAMP)* **21**, 645–647 (1970)
- Fang, T.; Yao, S.; Pop, I.: Flow and heat transfer over a generalized stretching/shrinking wall problem—exact solutions of the Navier-Stokes equations. *Int. J. Nonlinear Mech.* **46**(9), 1116–1127 (2011)
- Banks, W.H.H.: Similarity solutions of the boundary layer equations for a stretching wall. *J. Mécan Theor. Appl.* **2**, 375–392 (1983)
- Magyari, E.; Keller, B.: Exact solutions for self-similar boundary-layer flows induced by permeable stretching surfaces. *Eur. J. Mech. B Fluids* **19**, 109–122 (2000)
- Liao, S.J.; Pop, I.: Explicit analytic solution for similarity boundary layer equations. *Int. J. Heat Mass Transfer* **47**, 75–85 (2004)
- Carragher, P.; Crane, L.J.: Heat transfer on a continuous stretching sheet. *J. Appl. Math. Mech. (ZAMM)* **62**, 564–565 (1982)
- Grubka, J.L.; Bobba, K.M.: Heat transfer characteristics of a continuous stretching surface with variable temperature. *ASME J. Heat Transfer* **107**, 248–250 (1985)
- Dutta, B.K.; Roy, P.; Gupta, A.S.: Temperature field in flow over a stretching sheet with uniform heat flux. *Int. Commun. Heat Mass Transfer* **12**, 89–94 (1985)
- Gupta, P.S.; Gupta, A.S.: Heat and mass transfer on a stretching sheet with suction or blowing. *Can. J. Chem. Eng.* **55**, 744–746 (1977)
- Bataller, R.C.: Similarity solutions for flow and heat transfer of a quiescent fluid over a nonlinearly stretching surface. *J. Mater. Process. Tech.* **203**, 176–183 (2008)
- Afzal, N.: Momentum transfer on power law stretching plate with free stream pressure gradient. *Int. J. Eng. Sci.* **41**, 1197–1207 (2003)
- Weidman, P.D.; Kubitschek, D.G.; Davis, A.M.J.: The effect of transpiration on self-similar boundary layer flow over moving surfaces. *Int. J. Eng. Sci.* **44**, 730–737 (2006)
- Ishak, A.; Nazar, R.; Pop, I.: Flow and heat transfer characteristics on a moving flat plate in a parallel stream with constant surface heat flux. *Heat Mass Transfer* **45**, 563–567 (2009)
- Bataller, R.C.: Radiation effects for the Blasius and Sakiadis flows with a convective surface boundary condition. *Appl. Math. Comput.* **206**, 832–840 (2008)
- Turkylmazoglu, M.: Heat and mass transfer of MHD second order slip flow. *Comput. Fluids* **70**, 426–434 (2013)
- Andersson, H.I.; Hansen Olav, R.; Holmedal, B.: Diffusion of a chemically reactive species from a stretching sheet. *Int. J. Heat Mass Transfer* **37**(4), 659–664 (1994)
- Takhara, H.S.; Chamkha, A.J.; Nath, G.: Flow and mass transfer on a stretching sheet with a magnetic field and chemically reactive species. *Int. J. Eng. Sci.* **38**(12), 1303–1314 (2000)
- Akyildiz, F.T.; Bellout, H.; Vajravelu, K.: Diffusion of chemically reactive species in a porous medium over a stretching sheet. *J. Math. Anal. Appl.* **320**(1), 322–339 (2006)
- Ziabakhsh, Z.; Domairry, G.; Bararnia, H.; Babazadeh, H.: Analytical solution of flow and diffusion of chemically reactive species over a nonlinearly stretching sheet immersed in a porous medium. *J. Taiwan Inst. Chem. Eng.* **41**(1), 22–28 (2010)
- Pal, D.; Mondal, H.: Effects of Soret Dufour, chemical reaction and thermal radiation on MHD non-Darcy unsteady mixed convective heat and mass transfer over a stretching sheet. *Commun. Nonlinear Sci. Numer. Simul.* **16**(4), 1942–1958 (2011)
- Khan, W.A.; Pop, I.M.: Effects of homogeneous-heterogeneous reactions on the viscoelastic fluid toward a stretching sheet. *J. Heat Transfer* **134**(6), 064506 (2012)
- Bhattacharyya, K.; Mukhopadhyay, S.; Layek, G.C.: Unsteady MHD boundary layer flow with diffusion and first order chemical reaction over a permeable stretching sheet with suction or blowing. *Chem. Eng. Commun.* **200**, 379–397 (2013)
- Nellis, G.; Klein, S.: Heat Transfer. Cambridge University Press; 2008 [chapter 9, p. E23–5].
- Lienhard, IV J.H.; Lienhard, V J.H.: A Heat Transfer Textbook, 3rd ed. Cambridge, MA: Phlogiston Press; 2005 [p. 662–3].
- Acrivos, A.: The asymptotic form of the laminar boundary-layer mass-transfer rate for large interfacial velocities. *J. Fluid Mech.* **12**(3), 337–357 (1962)
- Spalding, D.B.: Mass transfer in laminar flow. *Proc. R. Soc. Lond. A* **221**, 78–99 (1954)
- Siddheshwar, P.G.; Mahabaleshwar, U.S.: Effects of radiation and heat source on MHD flow of a viscoelastic liquid and heat transfer over a stretching sheet. *Int. J. Non-Linear Mech.* **40**(6), 807–820 (2005)
- Mahabaleshwar, U.S.; Nagaraju, K.R.; Vinay Kumar, P.N.; Kelson, N.A.: An MHD Navier’s slip flow over axisymmetric linear stretching sheet using differential transform method. *Int. J. Appl. Comput. Math.* **4**(1), 30 (2017)
- Mahabaleshwar, U.S.; Vinay Kumar, P.N.; Sheremet, M.: Magnetohydrodynamics flow of a nanofluid driven by a stretching/shrinking sheet with suction. *Springerplus* **5**(1), 1901 (2016)
- Mahabaleshwar, U.S.; Nagaraju, K.R.; Sheremet, M.A.B.; D & Lorenzini, E.: Mass transpiration on Newtonian flow over a porous stretching/shrinking sheet with slip. *Chin. J. Phys.* **63**, 130–137 (2020)
- Mahabaleshwar, U.S.; VinayKumar, P.N.; Nagaraju, K.R.; Gabriella, B.; Nayakar, R.S.N.: A new exact solution for the flow of a fluid through porous media for a variety of boundary conditions. *Fluids* **4**(3), 125 (2019)
- Yadav, D.; Mahabaleshwar, U.S.; Wakif, A.; Chand, R.: Significance of the inconstant viscosity and internal heat generation on the occurrence of Darcy-Brinkman convective motion in a couple-stress fluid saturated porous medium: an exact analytical solution. *Int. Commun. Heat Mass Transfer* **122**, 105165 (2021)
- Xenos, M.A.; Petropoulou, E.N.; Siokis, A.; Mahabaleshwar, U.S.: Solving the nonlinear boundary layer flow equations with pressure gradient and radiation. *Symmetry* **12**(5), 710 (2020)
- Mahabaleshwar, U.S.; Nagaraju, K.R.; Vinay Kumar, P.N.; NdiAzese, M.: Effect of radiation on thermosolutal Marangoni convection in a porous medium with chemical reaction and heat source/sink. *Phys. Fluids* **32**(11), 113602 (2020)
- Shah, N.A.; Khan, I.: Heat transfer analysis in a second grade fluid over and oscillating vertical plate using fractional Caputo-Fabrizio derivatives. *Eur. Phys. J. C* **76**, 362 (2016)



41. Ali, F.; Saqib, M.; Khan, I.; Sheikh, N.A.: Application of Caputo-Fabrizio derivatives to MHD free convection flow of generalized Walters'-B fluid model. *Eur. Phys. J. Plus* **131**, 377 (2016)
42. Sheikh, N.A.; Ali, F.; Saqib, M.; Khan, I.; Jan, S.A.A.; Alshomrani, A.S.; Alghamdi, M.S.: Comparison and analysis of the Atangana-Baleanu and Caputo-Fabrizio fractional derivatives for generalized Casson fluid model with heat generation and chemical reaction. *Results Phys.* **7**, 789–800 (2017)
43. Khalid, A.; Khan, I.; Khan, A.; Shafie, S.: Unsteady MHD free convection flow of Casson fluid past over an oscillating vertical plate embedded in a porous medium. *Eng. Sci. Technol. Int. J.* **18**(3), 309–317 (2015)
44. Sowmya, G.; Gireesha, B.J.; Animasaun, I.L.: Nehad Ali Shah, Significance of buoyancy and Lorentz forces on water-conveying iron(III) oxide and silver nanoparticles in a rectangular cavity mounted with two heated fins: heat transfer analysis. *J. Therm. Anal. Calorim.* **144**, 2369–2384 (2021)

